Ultrasonics Sonochemistry 18 (2011) 310–317

Contents lists available at ScienceDirect

Ultrasonics Sonochemistry

journal homepage: www.elsevier.com/locate/ultsonch

The effect of high intensity ultrasound on the loading of Au nanoparticles into titanium dioxide

Valentina Belova *, Tatiana Borodina, Helmuth Möhwald, Dmitry G. Shchukin

Max-Planck Institute of Colloids and Interfaces, D14476 Potsdam, Germany

ARTICLE INFO

Article history:
Received 9 December 2009
Received in revised form 23 June 2010
Accepted 24 June 2010
Available online 1 July 2010

Keywords:
Cavitation
Nanocomposite
Mesoporous materials
Titanium dioxide
Photocatalyst

ABSTRACT

Novel metal/semiconductor nanocomposites have been synthesized from pre-formed components by applying high intensity ultrasound irradiation. Positively and negatively charged Au nanoparticles were intercalated into mesoporous TiO_2 by sonication. The synthesized nanocomposites with implanted gold nanoparticles possess a narrow pore-size distribution around 7 nm and a large surface area of about 210 m^2/g. The intercalation of the Au nanoparticles into the TiO_2 framework depends on the charge of the Au nanoparticles, time and amplitude of ultrasonic treatment. The experiments show that at 20 min of ultrasonic irradiation the volume fraction of the negatively charged Au nanoparticles intercalated into TiO_2 is 15%. By contrast, at the same time, 8.1% of positively charged Au nanoparticles with a diameter of about 6–7 nm enters into the TiO_2 matrix.

The characterization of the samples was carried out by X-ray diffraction, transmission electron microscopy, high-resolution transmission electron microscopy, scanning electron microscopy, Fourier transform infrared measurements and BET analysis. The structure of TiO_2 was not considerably affected by the intercalation of the Au nanoparticles. TiO_2 doped with negatively charged Au nanoparticles presented a higher photocatalytic activity (75 wt.%) than TiO_2 loaded with positively charged Au nanoparticles (62 wt.%), because of an enlarged surface area and quantity of Au nanoparticles in titania.

1. Introduction

Titanium dioxide (TiO_2) finds different application as a pigment, in sunscreens and other optical devices, coatings, paints, toothpaste, cosmetics, etc. [1–5]. Moreover, this material is widely used as a photocatalyst for the treatment of polluted water and air because it possesses high photosensitivity, is non-toxic and chemically inert [6–8]. TiO_2 is an effective photocatalyst for organic pollutants under ultraviolet light irradiation [9,10]. The photocatalytic properties of TiO_2 can be improved by doping with other metal oxides [11]. The major outcome of the previous studies is that metal-doped TiO_2 can reduce the electron–hole recombination and increase the hydroxyl radical concentration on the surface of TiO_2, which, in turn, increases the photocatalytic activity of TiO_2 [12]. Particularly, TiO_2 loaded with Au nanoparticles possesses unique catalytic properties, which can be explained by the interaction of Au nanoparticles with TiO_2 via charge transfer between gold and titanium dioxide [13,14]. According to many studies [15,16]. Au nanoparticles loaded into TiO_2-semiconductors induce a shift in the Fermi level on the surface of the semiconductor to negative potentials. This improves the energetics of the nanocomposite and increases the efficiency of the interfacial charge-transfer process [17,18]. The photocatalytic activity of the Au–TiO_2 nanocomposites depends on the method of preparation and dispersion of the Au nanoparticles into the TiO_2 matrix. Furthermore, the size and morphology of the Au nanoparticles greatly influence the catalytic properties of the nanocomposites. The greater shift in the Fermi level observed with smaller Au nanoparticles (3–5 nm) is reflected in greater photocatalytic reduction efficiency and higher photocurrent generation [17,19,20].

Different methods have been investigated to synthesize Au–TiO_2 composites depending on the materials and processing techniques. These include: reduction of Au nanoparticles in the presence of TiO_2 particles, sol–gel processing [17,21], the deposition–precipitation method [22], gas-phase grafting [23], ion implantation [24], UV-photolysis [25,26] among others. For example, semiconductor/metal composite nanoparticles synthesized by chemically reducing $HAuCl_4$ on the surface of pre-formed TiO_2 nanoparticles exhibit radical scavenging activity against DPPH radicals (1,1-diphenyl-2-picrylhydrazyl) [19]. The authors showed that the size of gold nanoparticles, as well as their catalytic activity, was significantly affected by the preparation methods and the type of TiO_2 supports. Also, nanocomposites consisting of Au and TiO_2 nanocrystals have been

* Corresponding author. Tel.: +49 0 331 567 9235; fax: +49 0 331 567 9202.
E-mail address: Valentina.Belova@mpikg.mpg.de (V. Belova).

1350-4177/$ - see front matter © 2010 Elsevier B.V. All rights reserved.
doi:10.1016/j.ultsonch.2010.06.012

synthesized through sol–gel reactions of titanium tetraisopropoxide with hydrogen tetrachloroaurate in the presence of copolymer as the template to direct the formation of nanostructured photocatalysts [13]. The resulting Au nanoparticles with diameter 50–120 nm were adsorbed on the TiO_2 surface. Another technique demonstrated in Ref. [7] shows that Au nanoparticles were embedded into the titania framework by a multicomponent assembly approach, where surfactant, titania and gold composed clusters were cooperatively assembled in a one step process.

Ultrasonic irradiation influences the formation of nanocomposites [27–30]. It is known that in liquids cavitation as a result of ultrasonic irradiation distorts the system integrity caused by the growth, the oscillation and the collapse of gas-bubbles. In heterogeneous systems (liquid–solid), the high-speed shock waves and microjets may induce surface damage and promote the penetration of the particles into the matrix material [31–33]. The effect of ultrasonic irradiation on the nanocomposite formation depends on the temperature, pressure, frequency and power of the sonoreactor and the concentration of the components.

In the present work we have developed a simple way to fabricate mesoporous nanocomposites with different loading level of Au nanoparticles. These composites are obtained by applying high-intensity ultrasonic irradiation on the positively charged titanium dioxide in the presence of Au nanoparticles. We focused on the coupled effect of differently charged Au nanoparticles and ultrasonic irradiation on the nanocomposite formation. It has been found that the intercalation of Au nanoparticles into a TiO_2 matrix under high-intensity ultrasonic irradiation (20 kHz, 51.3 W/cm^2) can be efficient for both positively and negatively charged Au nanoparticles. With positively charged gold, sonication can promote the intercalation of nanoparticles by overcoming the repulsion from TiO_2. Approximately 20–30 min of ultrasonic irradiation is an appropriate time for the formation of Au–TiO_2 nanocomposites. The loading value of the gold nanoparticles into TiO_2 is strongly dependent on both time and power of the applied ultrasonic treatment. Nanocomposites fabricated with negatively charged gold nanoparticles have the highest loading rate (15%) which is obtained at 20 min of sonication.

2. Experimental section

2.1. Materials

The hydrogen tetrachloroaurate (III) (99.999%), sodium borohydride (98%), tetraoctylammonium bromide (98%), 4-(dimethylamino) pyridine (99%), potassium perchlorate, sodium acetate, Triton X-100 (TX-100) and ethylenediaminetetraacetic acid (EDTA) were purchased from Sigma–Aldrich, Germany. The titanium (IV) *n*-butoxide (98%) and methyl orange were purchased from Alfa Aesar, Germany. Ethanol was purchased from VWR International S.A.S., France. All aqueous solutions were made using deionised Millipore Milli-Q water.

2.2. Characterization methods

UV–vis spectra were measured by a Varian CARY 50 UV–vis spectrophotometer. X-ray diffraction of the samples was studied on a Bruker AXS – D8 ADVANCE X-ray diffractometer and on a Nanostar Bruker AXS diffractometer. TEM and HRTEM studies were carried out on a JEOL-JEM 100 and Philips CM 200-FEG (operated at 200 kV) microscopes, respectively. Scanning electron microscopy was performed with a Gemini Leo 1550 instrument to study the morphology of nanocomposites. Nitrogen adsorption and desorption isotherms were measured at 196 °C using a Micrometrics Gemini 2375 analyzer after degassing of the samples at 120 °C for 1 h. The surface area was calculated from the linear part of the BET plot. The pore-size distribution was estimated by the Barrett–Joyner–Halenda (BJH) model involving the use of the Halsey equation [34]. The Fourier transform infrared measurements were carried out with a Bruker Hyperion 2000 IR spectrometer equipped with a 158 IR objective and MCT detector at room temperature in KBr pellets. The samples were crushed and blended with potassium bromide. For each sample, 2.5 mg of composites and 508 mg of KBr were weighed and then ground in an agate mortar for 10 min before making the pellets. Spectra were taken with 2 cm^{-1} resolution in a wavenumber range from 4000 to 400 cm^{-1}.

2.3. Synthesis of the Au nanoparticle/TiO_2 nanocomposite

Mesoporous titanium dioxide was prepared by using the hydrolysis condensation method [35]. The non-ionic surfactant Triton X-100 (TX-100) has been used as a template, which was easily removed by washing the precipitate with water and ethanol at room temperature. TX-100 was mixed with titanium (IV) *n*-butoxide (TBOT), followed by addition of absolute ethanol under stirring. Then water was added drop-wise under continuous stirring, which caused the immediate precipitation of a white solid. The molar composition of the reaction mixture was TBOT:TX-100:EtOH:-H_2O = 2:1:82.6:934. The mixture was left overnight at ambient temperature for 24 h and further aged at 80 °C for another 24 h. The product was collected by suction filtration, and then washed with ethanol: water solution (1:1) under stirring. Synthesized TiO_2 was dialyzed against pure water for removing the rest of the polymer.

The positively charged Au nanoparticles were synthesized by using the Brust two-phase method [36] as described in a previous study [32]. The gold nanoparticles modified by DMAP (dimethylamino)pyridine) are very stable over a long time (i.e., 4 months) in aqueous solution without any sign of agglomerates. They have a diameter of approximately 6 ± 0.5 nm. The negatively charged Au nanoparticles were synthesized by employing the procedure consisting of the reduction of chloroauric acid (CAA) by the disodium salt of ethylenediaminetetraacetic acid (EDTA) and sodium borohydride at room temperature and intense stirring [37]. These Au nanoparticles are also very stable and have a diameter similar to that of DMAP–Au particles.

The synthesized Au colloid solution (8.5 wt.%) was added to 0.05 g TiO_2 with vigorous stirring. The solution was then transferred to a sonication flask and sonicated for different times. The precipitated nano-Au intercalated product was separated by centrifugation, washed with water, and dried under vacuum overnight. Afterward, the samples were calcinated under air atmosphere at 350 °C for 3.5 h to finalize the nanocomposite production.

2.4. Ultrasonic treatment

A slurry of Au colloid solution and TiO_2 particles was ultrasonically irradiated at different sonication times (5, 10, 20, 30, 40 and 60 min) using a direct-immersion ultrasonic horn (ultrasonic processor UIP1000hd provided by Hielscher Ultrasonics). The experiments were carried out at an excitation frequency of 20 kHz with different power densities of ultrasound (29, 40, 51.3 W/cm^2). The temperature of the sonicated solution was controlled using a cooling system and kept between 35 and 40 °C. This temperature is favorable for producing a high cavitation field which greatly accelerated the incorporation of Au nanoparticles into TiO_2. 51.3 W/cm^2 was found to be the most appropriate power density of ultrasound for achieving the highest loading efficiency of Au nanoparticles intercalated into the TiO_2 matrix. By reducing the power density to 29 W/cm^2, the incorporation time was significantly increased.

Therefore, all results presented henceforth used a power density of 51.3 W/cm^2.

2.5. Evaluation of the photocatalytic efficiency of Au–TiO_2

The photocatalytic activity of the specimens was determined by photo degradation of methyl orange in water under UV-light. The nanocomposite (0.03 g) was dispersed in 70 ml of methyl orange aqueous solution (25 mg/L) in each experiment. The reactor was illuminated with a UV lamp (UV lamp TO 150, Heraeus 150 W, peak intensity at λ = 303 nm). The lamp emitted light from above the sample without any cover. The suspension was constantly stirred for 30 min in the dark before irradiation to reach equilibrium adsorption of methyl orange to the TiO_2 surface. During irradiation, the sample in the photoreactor was magnetically stirred to maintain a homogeneous suspension. A probe was collected and centrifuged at regular time intervals of irradiation (every 30 min), and the methyl orange concentration was measured using a Varian CARY 50 UV–vis spectrometer at 465 nm, which is the maximum absorption wavelength of methyl orange. The results were corrected for the decomposition of the methyl orange in the absence of catalysts and for adsorption of methyl orange on the TiO_2 surface.

3. Results and discussions

3.1. Microscopic characterisation (TEM, HRTEM, SEM)

TEM analysis was used in order to investigate the morphology of the synthesized TiO_2 and Au–TiO_2 nanocomposites. Fig. 1(a–c) shows a micrograph of the synthesized TiO_2 at low and high magnification. As it can be seen, most of the TiO_2 particles are spherical with a particle size of about 15–25 nm. The HRTEM image of pure TiO_2 (Fig. 1c) established the presence of anatase lattice fringes. This demonstrates that particles with anatase structure are connected to each other to form a mesoporous crystalline framework.

The TEM of Au–TiO_2 loaded from a positively charged gold colloid solution illustrates dispersion into the TiO_2 matrix (Fig. 1d–f) under sonication. Ultrasonic irradiation allows overcoming the repulsion from the equally charged TiO_2 and gold nanoparticles, promoting the intercalation of nano-gold into TiO_2. After sonication and further calcinations, the shape of the gold nanoparticles is spherical, with a diameter of 6–7 nm. The particle size under ultrasonic irradiation increased due to the decomposition of a fraction with smaller particles. By comparing the HRTEM of TiO_2

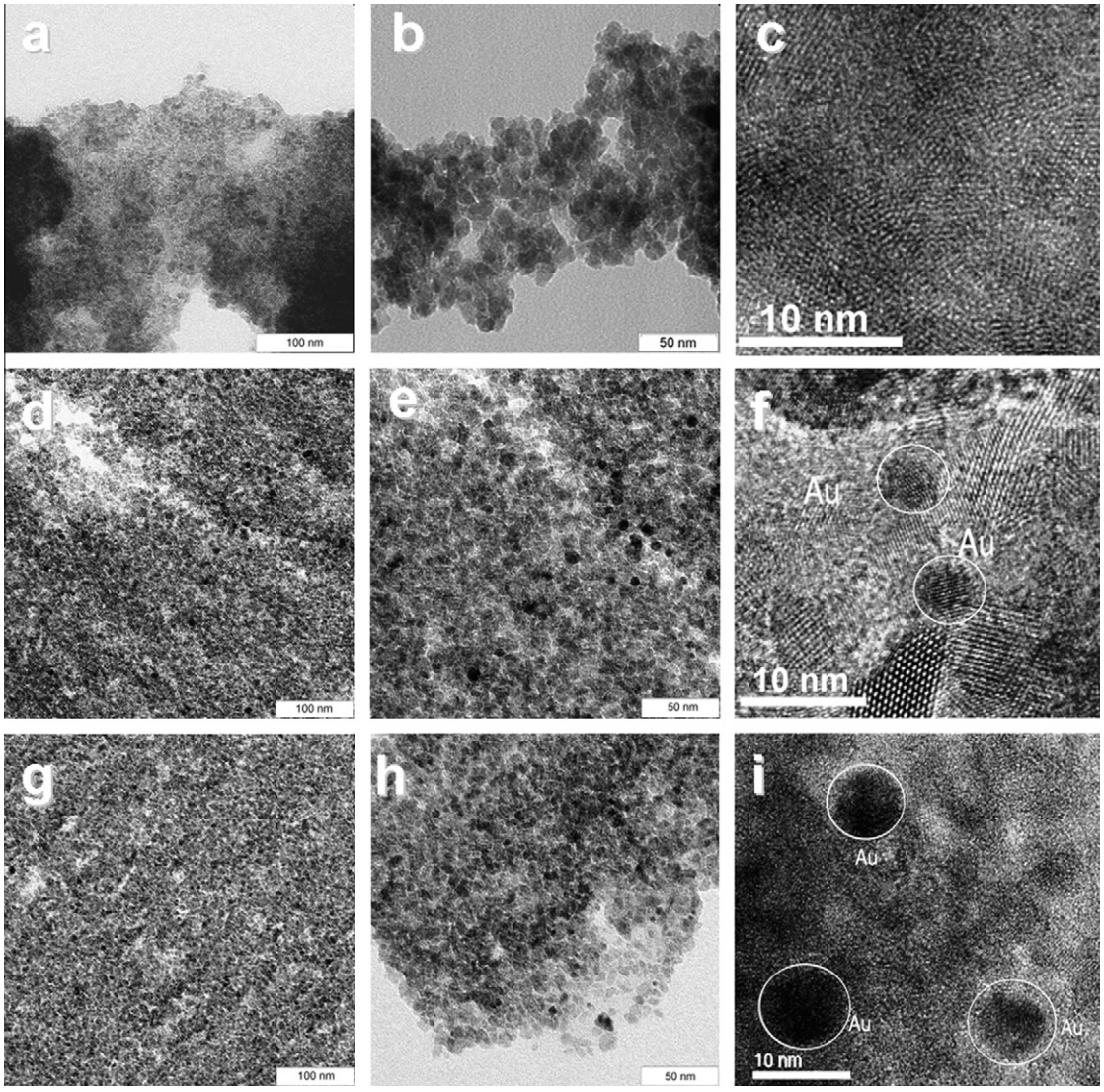

Fig. 1. TEM and HRTEM images of: (a–c) initial TiO_2; (d–f) Au–TiO_2 loaded with positively charged Au nanoparticles at 30 min of sonication; (g–i) Au–TiO_2 loaded with negatively charged Au nanoparticles at 20 min of sonication. The circles in f, i indicate Au nanoparticles.

(Fig. 1c) and Au–TiO_2 (Fig. 1f) it can be seen that the Au nanoparticles are well distributed within the framework.

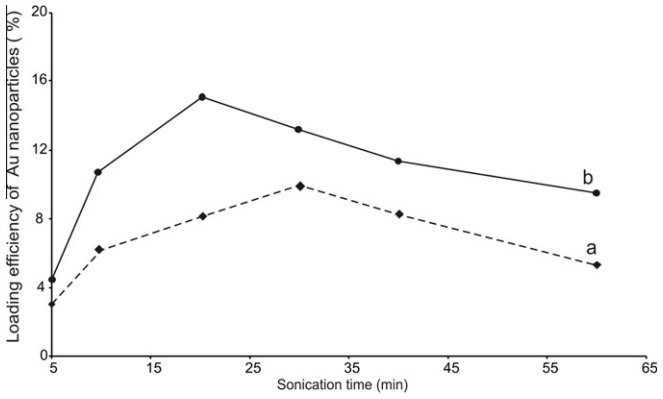

Fig. 2. Plot of the loading efficiency of Au nanoparticles in the TiO_2 matrix as a function of the sonication time: (a) – TiO_2 loaded with positively charged Au nanoparticles; (b) – TiO_2 loaded with negatively charged Au nanoparticles.

The amount of Au nanoparticles loaded into TiO_2 is henceforth referred to as the volume fraction [38] (see Supplementary material). After 10 min of sonication, the volume fraction of the Au nanoparticles is 6.5%. TEM micrographs of nanocomposites formed at different sonication times show that after 10 min of ultrasonic irradiation the content of Au nanoparticles in the TiO_2 matrix increased. At 30 min of sonication, the volume fraction of the Au nanoparticles in titanium dioxide is 10.4%. Longer sonication times result reduced the loading values of Au nanoparticles in titania.

In contrast, the TEM morphology of the nanocomposites loaded with negatively charged Au nanoparticles under sonication (Fig. 1g–i) indicates higher content of the gold nanoparticles in TiO_2. The main diameter of Au nanoparticles after ultrasonic intercalation is 5–7 nm. They are very well dispersed within the titania framework. Longer sonication times results in increasing contents of Au nanoparticles in the TiO_2 matrix. At 20 min of sonication the volume fraction of the Au nanoparticles is 15%.

The framework of TiO_2 and Au nanoparticles is highly crystalline as evidenced from the well resolved Au (1 1 1) (0.27 nm) and TiO_2 (1 0 1) (0.44 nm) crystalline lattices as shown in Fig. 1k. According to the plot of loaded content of Au nanoparticles in the TiO_2 matrix as a function of the sonication time (Fig. 2), one

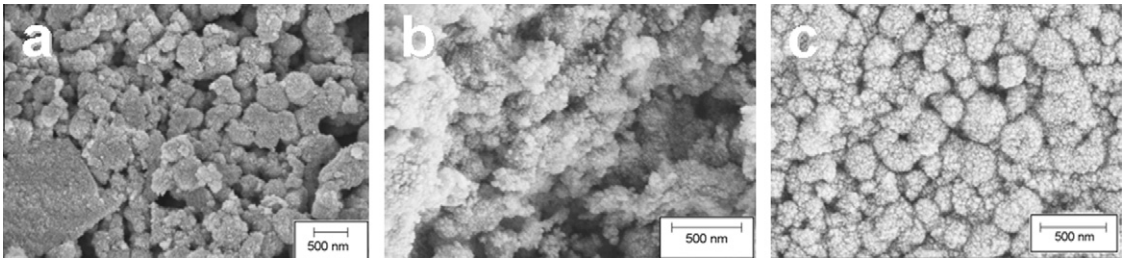

Fig. 3. SEM images of: (a) initial TiO_2; (b) Au–TiO_2 loaded with positively charged Au nanoparticles at 30 min of sonication; (c) Au–TiO_2 loaded with negatively charged Au nanoparticles at 20 min of sonication.

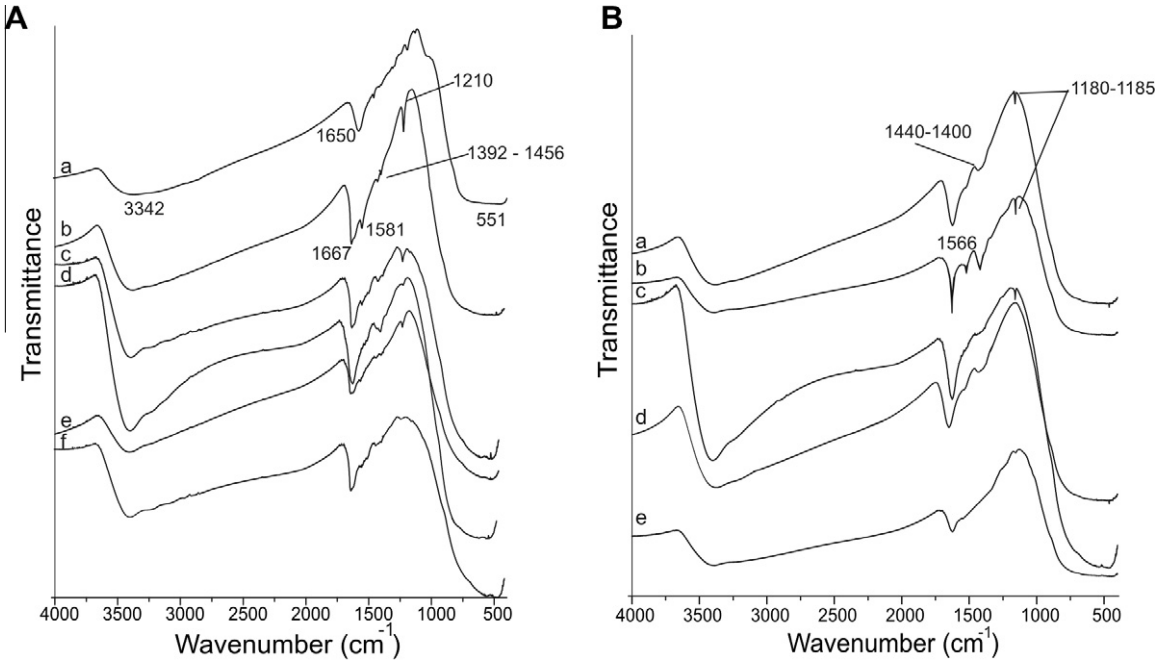

Fig. 4. A: FTIR spectra of the (a) initial TiO_2; (b–f) Au–TiO_2 loaded with positively charged Au nanoparticles: (b) Au–TiO_2 at 10 min of sonication; (c) Au–TiO_2 at 20 min of sonication; (d) Au–TiO_2 at 30 min of sonication; (e) Au–TiO_2 at 40 min of sonication; (f) Au–TiO_2 after calcination. B: Au–TiO_2 loaded with negatively charged Au nanoparticles: (a) Au–TiO_2 at 10 min of sonication; (b) Au–TiO_2 at 20 min of sonication; (c) Au–TiO_2 at 30 min of sonication, (d) Au–TiO_2 at 40 min of sonication; (e) Au–TiO_2 after calcination. All spectra were shifted along the transmittance axis for clarity but measured with the same sensitivity.

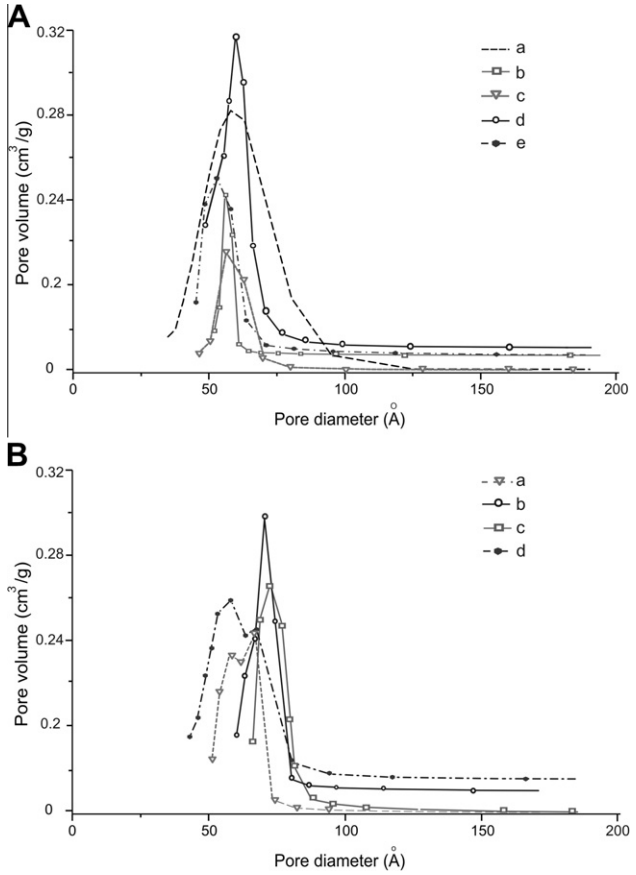

Fig. 5. A: Pore-size distribution of: (a) initial TiO_2; (b–e) Au–TiO_2 loaded with positively charged Au nanoparticles: (b) Au–TiO_2 at 10 min of sonication; (c) Au–TiO_2 at 20 min of sonication, (d) Au–TiO_2 at 30 min of sonication; (e) Au–TiO_2 at 40 min of sonication; B: pore-size distribution of Au–TiO_2 loaded with negatively charged Au nanoparticles: (a) Au–TiO_2 at 10 min of sonication; (b) Au–TiO_2 at 20 min of sonication, (c) Au–TiO_2 at 30 min of sonication; (d) Au–TiO_2 at 40 min of sonication.

can see that the TiO_2 obtained from negatively charged Au colloid solution is more filled than the TiO_2 intercalated from positively charged gold colloid solution; at 20 min of sonication, the content of positively charged Au nanoparticles is 1.8× lower than for the nanocomposite loaded with negatively charged Au nanoparticles.

The morphology of composites loaded with Au nanoparticles is different from the initial TiO_2 (Fig. 3). The particle size of TiO_2 after ultrasonic intercalation of nano-gold is significantly reduced due to the destruction of agglomerates. A small particle size can provide a larger specific surface area and reduces electron–hole pair recombination, which results in improved photocatalytic efficiency [12].

3.2. FTIR measurement

The TiO_2 and Au–TiO_2 nanocomposites synthesized by ultrasonic irradiation are characterized with FTIR spectroscopy as shown in Fig. 4 and summarized in Table S2 (see Supplementary material). For the FTIR spectrum of the pure TiO_2 (Fig. 4A-a), the adsorption peak at 3400–3500 cm^{-1} is assigned to the O–H vibration of interacting hydroxyl groups and the symmetric and antisymmetric O–H modes of the molecular water coordinated to Ti^{4+} cations. Also, a broad and strong adsorption peak in a range of 400–800 cm^{-1} corresponds to the characteristic absorbance of TiO_2 due to the formation of an O–Ti–O network. All peaks related to the stretching vibrations of the functional groups of the TiO_2 are present on the spectra of Au–TiO_2 nanocomposites.

Table 1
Characteristics of TiO_2 and Au–TiO_2 nanocomposites.

Sample name	BET surface area (m^2/g)	Pore volume (cm^3/g)	Pore diameter (D) (nm)
Initial TiO_2	190.61 ± 1	0.27 ± 0.01	5.9 ± 0.01
TiO_2 loaded from positively charged Au nanoparticles			
Au–TiO_2 at 5 min of US	221.07 ± 1	0.23 ± 0.01	5.8 ± 0.01
Au–TiO_2 at 10 min of US	208.05 ± 1	0.24 ± 0.01	6.7 ± 0.01
Au–TiO_2 at 20 min of US	216.43 ± 1	0.29 ± 0.01	6.8 ± 0.01
Au–TiO_2 at 30 min of US	228.12 ± 1	0.32 ± 0.01	7.1 ± 0.01
Au–TiO_2 at 40 min of US	215.83 ± 1	0.25 ± 0.01	5.9 ± 0.01
Au–TiO_2 at 60 min of US	190.48 ± 1	0.19 ± 0.01	5.4 ± 0.01
TiO_2 loaded from negatively charged Au nanoparticles			
Au–TiO_2 at 5 min of US	257.31 ± 1	0.29 ± 0.01	6.1 ± 0.01
Au–TiO_2 at 10 min of US	220.78 ± 1	0.25 ± 0.01	6.7 ± 0.01
Au–TiO_2 at 20 min of US	234.93 ± 1	0.30 ± 0.01	7.4 ± 0.01
Au–TiO_2 at 30 min of US	217.35 ± 1	0.27 ± 0.01	7.2 ± 0.01
Au–TiO_2 at 40 min of US	193.22 ± 1	0.23 ± 0.01	6.7 ± 0.01
Au–TiO_2 at 60 min of US	181.74 ± 1	0.19 ± 0.01	6.0 ± 0.01

The presence of positively charged Au nanoparticles in TiO_2 was observed due to the appearance of the peaks related to DMAP (Fig. 4A). Comparing the initial spectrum (Fig. 4a) and the spectra of Au–TiO_2 (Fig. 4A b–e) indicates that the incorporation of Au nanoparticles leads to a weak shift of the TiO_2 bands to lower wave numbers. After 5 min of sonication the new peaks for Au–TiO_2 nanocomposites appear at ~1385, 1447 and at ~1520 cm^{-1}, corresponding to the CN single bond stretching and the ring distortion C–N stretch, respectively. The highest intensity of these peaks was observed for nanocomposites formed at 30 min of sonication. Longer ultrasonic irradiation reduces the intensity of the peaks and all peaks shift to lower wave numbers. After calcination (Fig. 4h), the peaks assigned to the stretching vibrations in pyridines (1385, 1447 and 1520 cm^{-1}) almost disappear.

Fig. 4B indicates that all characteristic bands of negatively charged Au nanoparticles are present between 700 and 1600 cm^{-1} and these are all found in the spectra of Au–TiO_2 nanocomposites. The main characteristic bands of the intercalated Au nanoparticles are assigned as follows: a new peak corresponding to the C–C–N bending in amines appears at ~1180 cm^{-1} even after 5 min of sonication. Furthermore, two additional peaks appear at ~1400 and 1440 cm^{-1} related to the COO^- symmetric stretch and OH bending in carboxylic acids respectively. The band at ~1566 cm^{-1} corresponds to the COO^- antisymmetric stretch. The maximum intensity of these new peaks is observed after 20 min of sonication, suggesting that the maximum quantity of Au nanoparticles is loaded into TiO_2. Since titanium is a transition metal, it tends to form coordination compounds with the nitrogen atoms in the EDTA molecule. Therefore, the strong interaction is likely due to the interaction of titanium and nitrogen in the EDTA molecule. Moreover, the peaks persist even under a long sonication period (40–60 min), indicating that the TiO_2 is saturated with Au nanoparticles. The action of hydrogen bonding between TiO_2 and Au nanoparticles contributes to the shift of the bands to lower wave numbers. Longer ultrasonic irradiation also promotes merging of two peaks at 1400 and 1440 cm^{-1} into one broad peak corresponding to the intercalation of Au nanoparticles into TiO_2.

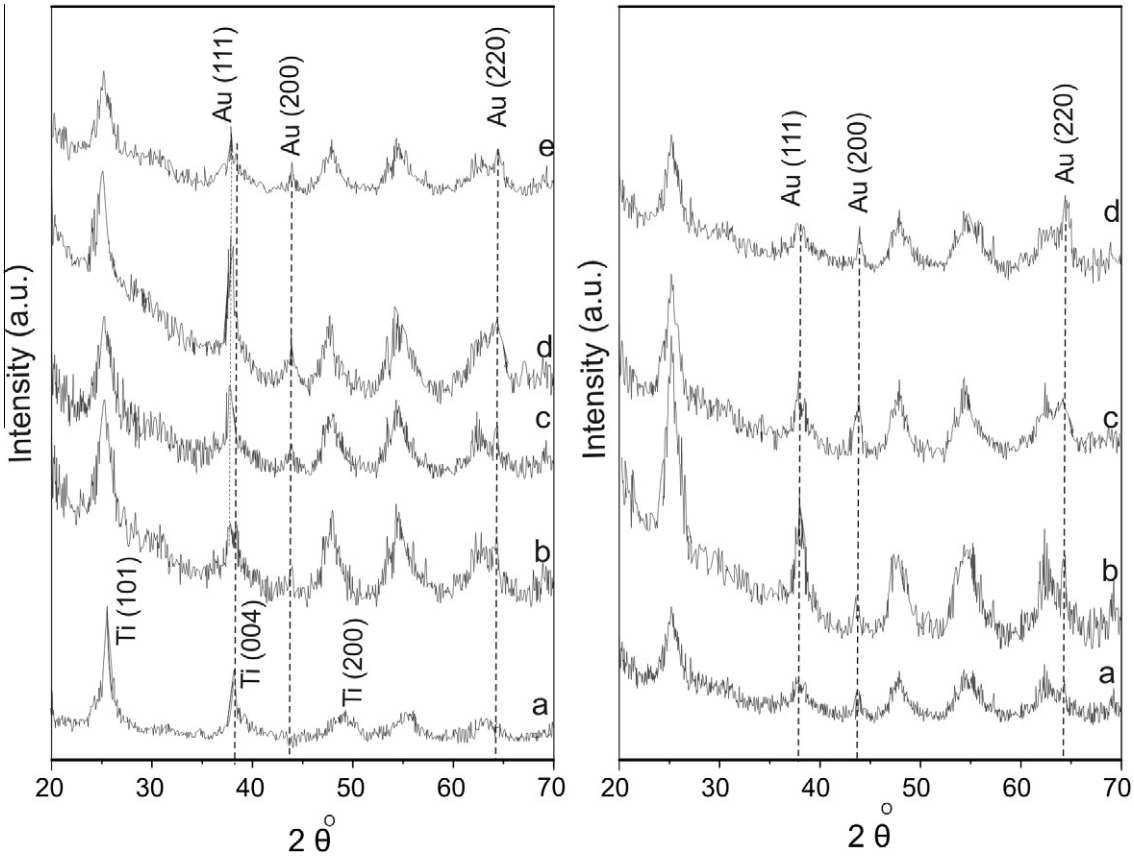

Fig. 6. *Left:* X-ray diffraction pattern of the (a) initial TiO_2; (b–e) Au–TiO_2 loaded with positively charged Au nanoparticles: (b) Au–TiO_2 at 10 min of sonication; (c) Au–TiO_2 at 20 min of sonication; (d) Au–TiO_2 at 30 min of sonication, (e) Au–TiO_2 at 40 min of sonication. *Right:* X-ray diffraction isotherm of the Au–TiO_2 loaded with negatively charged Au nanoparticles: (a) Au–TiO_2 at 10 min of sonication; (b) Au–TiO_2 at 20 min of sonication; (c) Au–TiO_2 at 30 min of sonication, (d) Au–TiO_2 at 40 min of sonication.

3.3. BET measurements

Fig. S1 (see Supplementary material) and Fig. 5 display adsorption/desorption characteristics and pore-size distributions of pure TiO_2 and Au–TiO_2 nanocomposites. The isotherm plot of the synthesized TiO_2 sample belongs to the IV isothermal type with a hysteresis loop of relative pressure between 0.4 and 0.8 (Fig. S1), which means that a mesoporous structure was formed [34,35]. The BJH pore-size distribution shows a narrow peak at 5.8 nm. The structure parameters of the mesoporous titania are summarized in Table 1. It can be seen that the initial TiO_2 has a BET surface area of 190 m^2/g and pore volume of 0.27 cm^3/g.

The structure of the titania remains mesoporous after the ultrasonic insertion of the positively charged Au nanoparticles. The nanocomposite synthesized at 10 min of ultrasound treatment shows a distinct hysteresis loop of relative pressure between 0.5 and 0.9 in the adsorption curve (Fig. S1). With increasing time of ultrasonic irradiation the adsorption is increased. The highest value corresponds to the nanocomposite formed at 30 min of sonication. Specific surface area, pore size, and pore volume of the Au–TiO_2 composites, determined by the BET (N_2) method, are presented in Table 1. According to the values of the pore characteristic from Table 1, the BET surface area measured after gold intercalation is still large (Fig. S1, Table 1). However, the high pore volume of 0.32 m^3/g confirms that the porosity of the matrix is largely maintained during gold loading; hence the pore volume remains accessible.

According to the BET measurements, after the insertion of the negatively charged Au nanoparticles into the TiO_2, its surface area has increased at short sonication time. Longer sonication reduces the BET area to 217 m^2/g for nanocomposites formed at 30 min of sonication. The same result is observed for the pore volume and average pore diameter, which have been reduced as well (Fig. 5B, Table 1). Thus, the pore volume is partly blocked by the inserted gold nanoparticles. The BET results are in agreement with the TEM observations. The interaction of the gold particles between the mesopores and the outer surface can be easily explained as a result of the size of the gold nanoparticles, which is relatively increased during sonication (to 7 nm), in comparison to the average pore diameter of 6.7 nm. This result indicates that only the negatively charged Au nanoparticles (about 5 nm) are inserted into the mesopores.

3.4. X-ray diffraction

Fig. 6 displays the XRD pattern of pure TiO_2 and Au–TiO_2 nanocomposites. Diffraction peaks are observed at $2\theta = 25.27°$, 37.80° and 48.05° corresponding to the (1 0 1), (0 0 4) and (2 0 0) planes of the anatase mesostructure, respectively. The results are in a good agreement with previous research concerning the synthesis of TiO_2 particles [35]. After ultrasonic treatment of TiO_2 in the presence of Au nanoparticles, diffraction peaks appeared at $2\theta = 38.2°$ and 44.4°, 64.8° which correspond to the (1 1 1), (2 0 0) and (2 2 0) planes of crystalline Au. At 30 min of sonication, the Au–TiO_2 composite loaded from positively charged Au colloid solution has the diffraction peaks with the highest intensities (Fig. 5 Left). Furthermore, the produced nanocomposite exhibits the highest content of Au nanoparticles, whereas the TiO_2 crystallization is weakened. In this case, the size of Au nanoparticles cannot be properly evaluated

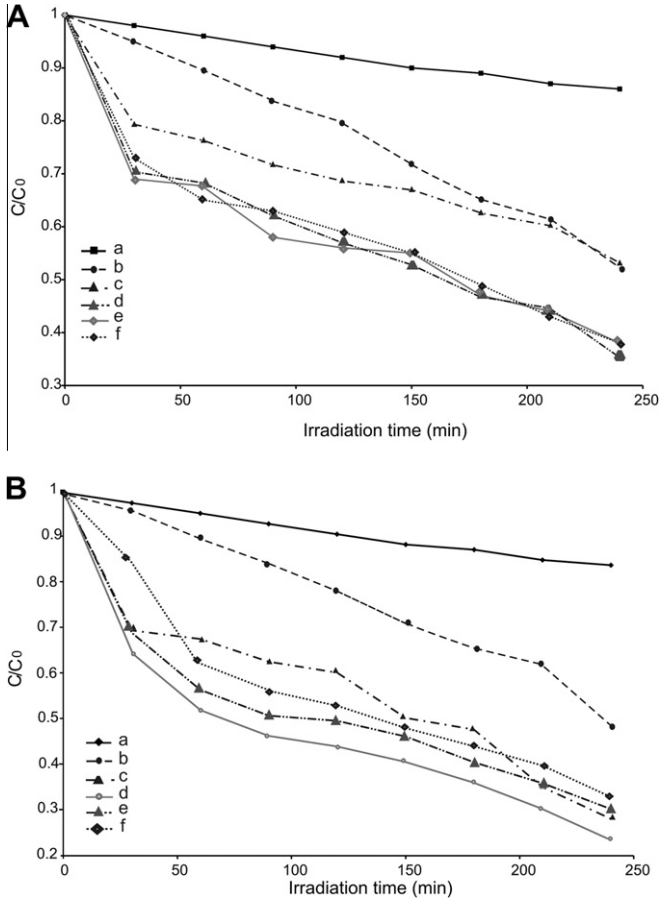

Fig. 7. A: Photocatalytic activity of the (a) blank–TiO_2; (b) Degussa P25; (c–f) Au–TiO_2 loaded with positively charged Au nanoparticles: (c) Au–TiO_2 at 10 min of sonication; (d) Au–TiO_2 at 30 min of sonication, (e) Au–TiO_2 at 40 min of sonication; (f) Au–TiO_2 at 60 min of sonication. B: Photocatalytic activity of the (a) blank–TiO_2; (b) Degussa P25; (c–f) Au–TiO_2 loaded with negatively charged Au nanoparticles: (c) Au–TiO_2 at 10 min of sonication; (d) Au–TiO_2 at 20 min of sonication, (e) Au–TiO_2 at 30 min of sonication, (f) Au–TiO_2 at 60 min of sonication.

with Scherrer's equation (Ref. [39]), because the strongest Au peak (1 1 1) is overlapped by a TiO_2 peak (0 0 4). Therefore the Au particle size was determined by TEM measurements. Longer sonication period shows a decrease of the peak intensity evidencing reduction of the content of gold nanoparticles inside the TiO_2. This result was also confirmed by BET, FTIR and TEM (see the paragraphs above). The same effect was observed in previous research [32,33], where after certain time of ultrasonic irradiation, the amount of loaded nanoparticles in the clay matrix is decreased. Likely, the mechanical force of the longer cavitation period partly distorts the TiO_2 structure and further loading by Au nanoparticles is reduced. Au–TiO_2 nanocomposites loaded with negatively charged Au nanoparticles show similar results (Fig. 6 Right). At 5, 10, 20 min of sonication the Au–TiO_2 shows gold diffraction peaks, which were detected in the patterns from the (1 1 1) and (2 0 0) reflections. The stronger and higher diffraction peak intensity corresponds to Au nanoparticles at 20 min of sonication due to the increasing content of Au nanoparticles in the TiO_2 matrix.

3.5. Photocatalytic efficiency of Au–TiO_2 nanocomposites

Fig. 7 shows the photocatalytic degradation of methyl orange for TiO_2 loaded with differently charged Au nanoparticles under ultrasonic irradiation. We used Degussa P25, a non-porous material formed by a mixture of anatase and rutile (80:20), as a reference substance for comparing the photocatalytic performances of TiO_2. The BET surface area of Degussa P25 is about 55 m^2/g and the average size of the particles is 30 nm. The formation of the Au–TiO_2 nanocomposites is strongly influenced by ultrasonic irradiation that subsequently influences their photocatalytic properties. The mechanism and scheme of the photocatalytic process are described in the Supplementary material (Fig. S2 and Eqs. 1–7).

Fig. 7A illustrates the photocatalytic activity of TiO_2 loaded from positively charged Au colloid solution. Curve (a) shows that in the absence of a photocatalyst the degradation of the methyl orange is slow under UV irradiation. Compared with Degussa P25 (Fig. 7A (curve b)), the nanocomposites show a significantly higher degradation rate of the methyl orange. The photocatalytic decomposition increases with irradiation time and reaches a maximum value at 30 min. 62% of methyl orange is degraded after 240 min of UV irradiation (Fig. 7A curve d), while at the same time only 48% of Degussa P25 is degraded. According to BET analyses, at this time the Au–TiO_2 nanocomposite has a bigger surface area. It is known that surface area of TiO_2 and amount of Au nanoparticles are among the dominant factors in the photocatalytic reaction [40]. Therefore this nanocomposite has the highest photocatalytic activity. However, with increasing sonication time up to 40–60 min the surface area and the loading rate of the nanocomposites become smaller; which leads to the lower photocatalytic efficiency (see results of BET analysis).

Fig. 7B shows the photocatalytic activity of Au–TiO_2 nanocomposites loaded from negatively charged Au colloid solution. 75% of methyl orange is degraded after 240 min of UV irradiation (Fig. 7B curve d). The nanocomposites formed with negatively charged Au nanoparticles exhibit better photocatalytic performance than TiO_2 nanocomposites loaded with positively charged Au nanoparticles. The limiting factors are the different surface area and loading values of the Au nanoparticles in TiO_2 which were formed during ultrasonic synthesis. The surface area and amount of Au nanoparticles of the nanocomposite loaded from negatively charged gold colloid solution at 20 min of sonication are higher than for the nanocomposite loaded from positively charged Au colloid solution. The enhanced photocatalytic activity of the Au–TiO_2 composites with UV treatment is most likely affected by the decrease of the electron/hole recombination rate due to special resolution of photo-generated charges between TiO_2 (photohole) and Au (photoelectron).

4. Conclusions

In summary, Au–TiO_2 nanocomposites with highly loaded yet dispersed Au nanoparticles in TiO_2 were synthesized in a simple way by involving high-intensity ultrasonic irradiation, which plays an indispensible role in nanocomposite formation. All analyses demonstrate that sonication promotes the incorporation Au nanoparticles into mesoporous TiO_2 independent of their charge. Nanocomposites prepared by ultrasound have high specific surface area, small particle size and good crystallinity. SEM studies show that the size of the TiO_2 nanoparticles is reduced due to the destruction of agglomerates. TiO_2 with smaller size provides a greater specific surface area and reduces electron–hole pair recombination, which results in improved photocatalytic efficiency. The FTIR spectra reveal the interaction between Au nanoparticles and titania. According to the XRD analysis, all nanocomposites have diffraction peaks assigned to anatase phase of TiO_2 and Au nanoparticles. The photocatalytic activity of Au–TiO_2 nanocomposites was examined via the photodegradation of aqueous methyl orange. The composites show high photocatalytic activity and they can find application as photocatalysts. TiO_2 loaded with Au nanoparticles could also be applicable for surface reaction devices and optoelectronic devices due to their good absorption properties [41,42].

This technique utilizes high-intensity ultrasonic irradiation as an energy source to facilitate the intercalation of nanoparticles into the TiO_2 matrix by reducing the reaction time, as well as significantly increasing the loading rates of Au nanoparticles. This provides a new method to fabricate photoactive materials. Sonication allows one to significantly improve the synthesis of Au–TiO_2 nanocomposites. The proposed method permits to control the loading rates of the noble nanoparticles and photocatalytic properties of the nanocomposites.

Acknowledgments

The work was supported by the EU FP7 NanoHy project, DAAD Germany–China project and by the Gay-Lussac/Humboldt Award to Helmuth Möhwald. We thank the Dr. Hartmann and Rona Pitschke for helping with TEM measurements. The authors also thank Dr. Dangsheng Su and Dr. Wei Zhang from the Fritz Haber Institute of the Max-Planck Society (Department of Inorganic Chemistry) for helping with HRTEM measurements.

Appendix A. Supplementary data

Supplementary data associated with this article can be found, in the online version, at doi:10.1016/j.ultsonch.2010.06.012.

References

[1] E. Cattaruzza, Nucl. Instrum. Methods Phys. Res., Sect. B 169 (2000) 141–155.
[2] H. Shinojima, J. Yumoto, S. Uesugi, Appl. Phys. Lett. 60 (1992) 298–300.
[3] S.A. Kumar, P.H. Lo, S.M. Chen, Nanotechnology 19 (2008) 7.
[4] G.S. Devi, T. Hyodo, Y. Shimizu, et al., Chem. Sens. 17 (2001) 291–293.
[5] D.E. Seong-Jim Kim, J. McKean, Mater. Sci. Lett. 17 (1998) 141–144.
[6] A.J. Bard, M.A. Fox, Acc. Chem. Res. 28 (1995) 141.
[7] H. Li, Z. Bian, J. Zhu, Y. Huo, H. Li, Y. Lu, J. Am. Chem. Soc. 129 (2007) 4538–4539.
[8] C. Laberty-Robert, M. Kuemmel, J. Allouche, C. Boissière, L. Nicole, D. Grosso, C. Sanchez, Mater. Chem. 18 (2008) 1216–1221.
[9] I.M. Arabatzis, T. Stergiopoulos, D. Andreeva, S. Kotova, S.G. Neophytides, P. Faralas, J. Catal. 220 (2003) 127–135.
[10] C. Randorn, J.T.S. Irvine, P. Robertson, Int. J. Photoenergy (2008) 6.
[11] H. Narayan, H. Alemu, L. Macheli, M. Thakurdesai, T.K. Rao, Nanotechnology 20 (2009) 8.
[12] J.M. Jung, M. Wang, E.J. Kim, S.H. Hahn, Vacuum 82 (2007) 827–832.
[13] A.A. Ismail, D.W. Bahnemann, I. Bannat, M. Wark, J. Phys. Chem. C 113 (2009) 7429–7435.
[14] J. Kim, D. Lee, J. Am. Chem. Soc. 129 (2007) 7706–7707.
[15] M. Jakob, H. Levanon, P.V. Kamat, Nano Lett. 3 (3) (2003) 353–358.
[16] A. Wood, M. Giersig, P. Mulvaney, J. Phys. Chem. B 105 (2001) 8810.
[17] V. Subramanian, E.E. Wolf, P.V. Kamat, J. Am. Chem. Soc. 126 (2004) 4943–4950.
[18] H.J. Kim, Y.G. Shul, H. Han, Stud. Surf Sci. Catal. 154 (2004) 581.
[19] R. Isono, T. Yoshimura, K. Esumi, J. Colloid Interf. Sci. 288 (2005) 177–183.
[20] L. Guczi, A. Beck, K. Frey, Gold Bull. 42 (2009) 5–12.
[21] Y. Hosoya, T. Suga, T. Yanagawa, Y. Kurokawa, J. Appl. Phys. 81 (1997) 1475–1480.
[22] J. Xu, Y. Sun, Y. Zhao, et al., Int. J. Photoenergy (2007) 7.
[23] M. Okumura, S. Tsubota, M. Haruta, J. Mol. Catal. 199 (2003) 73.
[24] C.M. Wang, Y. Zhang, V. Shutthanandan, S. Thevuthasan, G. Duscher, J. Appl. Phys. 95 (2004) 8185–8193.
[25] C.Y. Wang, L. Chen, T. Shen, J. Colloid Interf. Sci. 191 (1997) 464–470.
[26] T. Soejima, H. Tada, T. Kawahara, S. Ito, Langmuir 18 (2002) 4191–4194.
[27] K.S. Suslick, D.J. Casadonte, M.L.H. Green, M.E. Thompson, Ultrasonics 25 (1987) 56–59.
[28] K. Chatakondu, M.L.H. Green, M.E. Thompson, K.S. Suslick, J. Chem. Soc. Chem. Commun. 109 (1987) 900–901.
[29] W. Lim, Z. Zhong, A. Borgna, Chem. Phys. Lett. 471 (2009) 122–127.
[30] S. Anandan, M. Aschokkumar, Ultrason. Sonochem. 16 (2009) 316–320.
[31] K.S. Suslick, G.J. Price, Annu. Rev. Mater. Sci. 29 (1999) 295–326.
[32] V. Belova, H. Möhwald, D.G. Shchukin, Langmuir 24 (2008) 9747–9753.
[33] V. Belova, D.V. Andreeva, H. Möhwald, D.G. Shchukin, J. Phys. Chem. C 113 (2009) 5381–5389.
[34] S.J. Gregg, K.S. Sing, Adsorption, Surface Area and Porosity, 2nd ed., Academic Press, London, 1982.
[35] Y. Wang, Z.H. Jiang, Mater. Sci. Eng. B 128 (2006) 229–233.
[36] M. Brust, D. Bethell, D.J. Schiffrin, C. Kiely, J. Adv. Mater. 7 (1995) 795–797.
[37] A.M. Yaschenok, O.A. Inozemtseva, D.A. Gorin, B.N. Khlebtsov, Colloid J. 71 (2009) 422–429.
[38] D. Grigoriev, D. Gorin, G.B. Sukhorukov, A. Yashchenok, E. Maltseva, H. Möhwald, Langmuir 23 (2007) 12388–12396.
[39] P. Scherrer, R. Zsigmondy, Kolloidchemie, third ed., Otto Spamer, Leipzig, 1920, 394p.
[40] J. Wang, R.H. Li, Z.H. Zhang, Chem. Technol. Biotechnol. 82 (2007) 588–597.
[41] N. Chandrasekharan, P.Y. Kamat, J. Phys. Chem. B 104 (2000) 10851–10857.
[42] H. Tada, T. Mitsui, T. Kiyonaga, T. Akita, K. Tanaka, Nat. Mater. 5 (2006) 782–786.